Iowa State University
Digital Repository

Retrospective Theses and Dissertations | Iowa State University Capstones, Theses and Dissertations

1-1-2003

GaAs and InAs Hall effect devices for nondestructive evaluation

Micah Ray Decker
Iowa State University

Follow this and additional works at: https://lib.dr.iastate.edu/rtd

Recommended Citation

Decker, Micah Ray, "GaAs and InAs Hall effect devices for nondestructive evaluation" (2003). *Retrospective Theses and Dissertations*. 19940.
https://lib.dr.iastate.edu/rtd/19940

This Thesis is brought to you for free and open access by the Iowa State University Capstones, Theses and Dissertations at Iowa State University Digital Repository. It has been accepted for inclusion in Retrospective Theses and Dissertations by an authorized administrator of Iowa State University Digital Repository. For more information, please contact digirep@iastate.edu.

GaAs and InAs Hall effect devices for nondestructive evaluation

by

Micah Ray Decker

A thesis submitted to the graduate faculty

in partial fulfillment of the requirements of

MASTER OF SCIENCE

Major: Electrical Engineering

Program of Study Committee:
Gary Tuttle (Major Professor)
John Bowler
Alan Constant

Iowa State University

Ames, Iowa

2003

Graduate College

Iowa State University

This is to certify that the master's thesis of

Micah Ray Decker

has met the thesis requirements of Iowa State University

Signatures have been redacted for privacy

TABLE OF CONTENTS

ABSTRACT		v
CHAPTER 1. INTRODUCTION		
1.1	Motivation	1
1.2	The Hall Effect	4
1.3	Currently Available Technology	12
1.4	Material Growth	14
CHAPTER 2. DEVICE PATTERNS		
2.1	First Set of Masks	19
2.2	Second Set of Masks	22
2.3	Final Mask Set	26
CHAPTER 3. DEVICE FABRICATION		
3.1	Fabrication Process	29
3.2	First Layer Lithography	31
3.3	First Layer Etching	33
3.4	Second Layer Processing, Metallization	35
CHAPTER 4. TESTING OF DEVICES		
4.1	Measurement Procedures	40
4.2	Measurement Apparatus	43
CHAPTER 5. DEVICE CHARACTERIZATION		
5.1	Fabrication Results	46
5.2	Device Characterization Results	48
5.3	Hall Array Results	52

5.4 Conclusions 53

5.5 Future Work 55

APPENDIX. BLACK BOX S.O.P. 57

REFERENCES 58

ACKNOWLEDGMENTS 60

ABSTRACT

Nondestructive evaluation (NDE) is frequently used to examine components that experience significant stresses to ensure they are capable of safely performing their required tasks. The eddy-current technique of NDE utilizes an induced magnetic field to detect flaws or defects such as stress fractures in components. Semiconductor Hall sensors are one method for detecting magnetic fields induced by eddy-currents. While a single sensor can be used to detect the presence of a defect, an array of Hall sensors can potentially provide images of defects.

Single Hall devices and arrays were fabricated using bulk GaAs and InAs quantum wells to achieve well-controlled, high sensitivity devices. The quantum wells are used to control the sheet concentration of the material. Negative lithography and metal liftoff processes were used during fabrication. Individual Hall bars, van der Pauw devices, Hall strips, and arrays of Hall bars were fabricated and characterized. These devices were characterized by measuring mobility, carrier concentration, sensitivity, and temperature dependence. InAs quantum well device sensitivities were measured to be on the order of 56 V/A·T, which is much greater then InAs devices available commercially. The temperature dependence of the sensitivity of InAs quantum well devices was found to be –0.028 V/A·T per degree C.

CHAPTER 1: INTRODUCTION

1.1 Motivation

Nondestructive evaluation (NDE) is a very important tool in industry. It is especially significant in the testing and inspection of certain components that are vital to a larger machine. NDE is frequently used to examine components that experience significant stress to make sure they are capable of performing as required. One of the most obvious applications is the inspection of aircraft and spacecraft equipment. Being able to monitor components in such systems helps to reduce the risk of failure during operation. Reducing the amount of failures not only saves money, but can also save lives.

Inspection of metallic components can be done using a number of NDE techniques; visual, ultrasound, radiography, magnetic-particle, dye-penetrant and eddy-current [9]. Visual inspection is one of the most common techniques especially in finding surface defects. Most often a visual inspection is done with the naked eye or with the aid of a microscope. Visual inspections rely on the knowledge and ability of the person performing the inspection, which can make the inspection unreliable.

The ultrasound technique can be split into two different methods. Both methods allow inspection of defects that are located below the surface of the component. The first type of ultrasound is the transmission method. The transmission method uses the attenuation of ultrasonic waves passing through the sample to detect flaws [9]. The other type of ultrasound is pulse-echo. Pulse-echo is performed through the examination of the amplitude and time of flight of reflected ultrasonic waves [9].

The third type of NDE is radiography. Like ultrasound, there are also two methods of radiography. These two methods utilize X-rays and γ-rays. The difficult and dangerous

drawbacks of these types of inspections are the need for access to the component, bulky equipment, and the need to control the energy of the X-rays and γ–rays [9].

The fourth and fifth techniques are magnetic-particle inspection and dye-penetration. Magnetic-particle inspection (MPI) is a simple, non-quantitative technique that relies strongly on operator skill [9]. Although MPI is simple, it is only applicable to ferromagnetic materials thus limiting its use. Dye-penetration is very similar to MPI due to its use of a liquid, which penetrates surface cracks and then is developed and detected [9]. These two methods are most alike in their disadvantages. They both are messy and the results depend heavily on the skill of the person performing the inspection.

The last technique listed above is the eddy-current technique. The eddy-current technique utilizes an induced magnetic field to detect flaws or defects in components. Eddy-currents are produced in a metallic component by passing an alternating current through a coil placed near the surface of the component. While passing through the component, the eddy-currents interact with the metal. This interaction is dependent upon the composition and conductivity of the metal. When there is a defect or fracture in the metal sample, the composition and conductivity at that point change. This change alters the interaction of the eddy-currents, thus producing an alteration in the magnetic field inside and outside of the component. These defects are found by examination of the magnetic flux lines outside the component. As shown in the Fig. 1.1, where a crack or defect exists in the material, the flux lines are altered from what they would normally be without the defect.

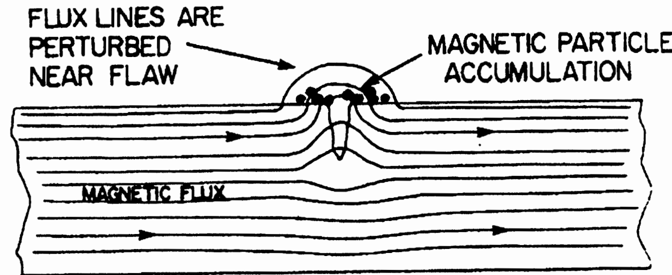

Figure 1.1. Magnetic flux lines around a surface crack within a specimen. From [1]

By looking at this diagram, it is easy to see how the magnetic field just outside the sample would be different in the presence of a defect.

Even though most often a number of the above mentioned tests are performed when inspecting a component, the main focus of this research is the study of the eddy-current method of inspection. In using this method to detect flaws, there must be a sensor to detect the eddy-currents. Hall sensors are extremely useful in detecting magnetic fields. A single Hall sensor can detect the presence of a crack in a component. Although the sensor will detect a crack, it will not provide sufficient information about the size and depth below the surface of the defect. For this reason an array of Hall devices is used to create an image of the eddy-currents in a specific area of the component.

Taking a Hall measurement from each device in an array while the probe is set in one place, allows an image to be created. This image is used to determine if there are any defects, mainly cracks or weak spots, within the specimen. If a change in magnetic field can be measured, the location of the crack can be determined. Furthermore, if the magnitude of change in the magnetic field can be measured, the size of the crack and the depth within the sample can also be determined. Using a computer program to visually display the numerical results from the array, the defects can be located and sizes determined. A group at Jenteck

Sensors, Inc. used an array of Hall sensors to create an image of the defects in a lapjoint [10]. Using the data from that array, a background reading was found and subtracted from the overall readings. These values were then inputted into an optical imaging system to display the image in the bottom half of Fig. 1.2.

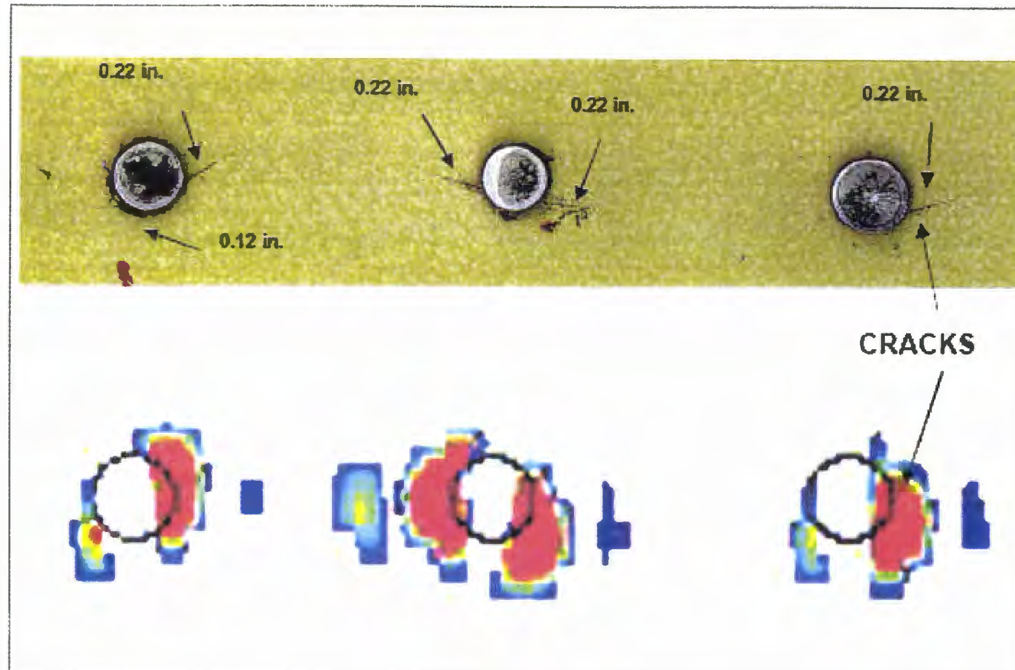

Figure 1.2. Hall array sensing image. From [10]

1.2 Hall Effect

The above description of the eddy-current technique demonstrates the need to find a method for measuring the change in the magnetic field at the surface of the specimen. There is one very simple device, which will allow for the measurement of a magnetic field. The theory behind this device is the Hall effect. The Hall effect is based on the Lorentz force law,

$$\vec{F} = q\left(\vec{v} \times \vec{B}\right), \tag{1.1}$$

where q is the charge, *v* is the velocity vector of the charge, and B is the magnetic field vector. Equation 1.1 describes the force an electron would experience due to the presence of a magnetic field. Hall devices can also be used in the converse manner. If a specific voltage is measured, the size of the magnetic field at that point can be calculated. The top view of a Hall device is shown in Fig. 1.3.

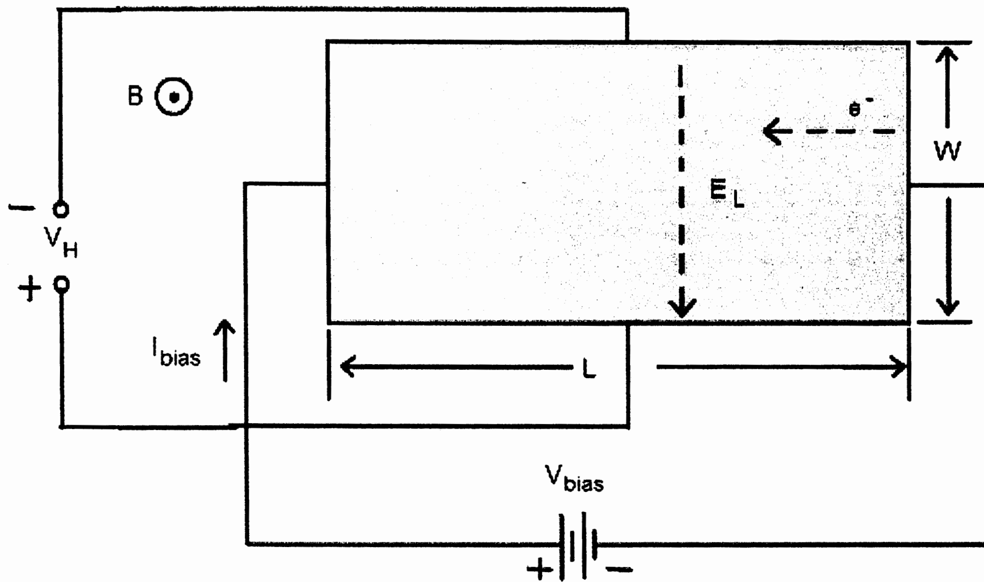

Figure 1.3. A rectangular Hall device. From [6]

The above diagram shows the effect of a magnetic field on the current passing through the device. As the strength of the magnetic field increases, the force on the electrons increases. To determine the output of a Hall device, it is necessary to first look at the current passing through the device. From this point, all symbols representing magnitudes and vector

directions can be seen in Fig. 1.3. From Fig. 1.3 the relationship between the bias current and bias voltage is derived and shown below as Eq. 1.2.

$$I_{bias} = \frac{V_{bias}}{R} \quad (1.2)$$

For the device shown in Fig. 1.3, the length of the device is denoted as L, the width as W, and the thickness by d. Using these parameters and Eq. 1.2, the resistance of the device can be formulated.

$$R = \frac{\rho L}{A} = \frac{L}{q\mu_n n W d} \quad (1.3)$$

In Eq. 1.3, ρ represents the resistivity of the sample, n is the electron concentration, and μ_n is the electron mobility. From the resistance, the resistivitiy of the sample can be calculated. The resistivitiy equation follows from Eq. 1.3.

$$\rho = \frac{1}{q\mu_n n} \quad (1.4)$$

The voltage drop applied across the length of the sample leads to an electric field in the sample given by Eq. 1.5.

$$E_L = \frac{V_{bias}}{L} \quad (1.5)$$

Before solving for the force applied to the electrons, it is necessary to know the velocity of the electrons in the sample. Equation 1.6 relates the electron mobility in the material to the

electron velocity in the material due to the electric field parallel to the dimension L of the device.

$$v_n = \mu_n E_L \tag{1.6}$$

Multiplying the electron velocity by the charge and the carrier concentration gives the current in the sample. Which then leads to the conductivity of the sample.

$$\sigma = q\mu_n n = \frac{1}{\rho} \tag{1.7}$$

Mobility is a measure of the carrier transport due to drift. In other words the mobility describes how electrons or holes move through a material when under the influence of an electric field. The characteristics of a material and its mobility will be discussed in more depth later.

When the applied magnetic field (B) is perpendicular to the plane of the Hall device, the Lorentz force simplifies to the following.

$$F_T = -q\mu_n E_L B \tag{1.8}$$

The above force bends the path of the electron toward one side of the sample depending on the direction of the magnetic field through the sample. The curvature in the path of the electron creates a charge imbalance across the device. This buildup of charge leads to a counter balancing Hall electric field (E_H),

$$E_H = \mu_n E_L B. \tag{1.9}$$

Substituting Eq. 1.9 Into Eq. 1.8 gives the force on the electron dependent upon the Hall electric field.

$$F_T = qE_H \tag{1.10}$$

Knowing the Hall electric field and the distance the electric field is applied across the Hall voltage can be found.

$$E_H = \frac{-V_H}{W} \tag{1.11}$$

Combining Eq. 1.5, Eq. 1.9, and Eq. 1.11, the Hall voltage across the device can be found.

$$V_H = \mu_n B \frac{W}{L} V_{bias} \tag{1.12}$$

Knowing how the Hall voltage relates to the electron mobility is an important consideration for material growth. When growing materials, another very common parameter to characterize the material is the carrier concentration. The mobility can be related to the carrier concentration or impurity concentration by the graph in Fig. 1.4.

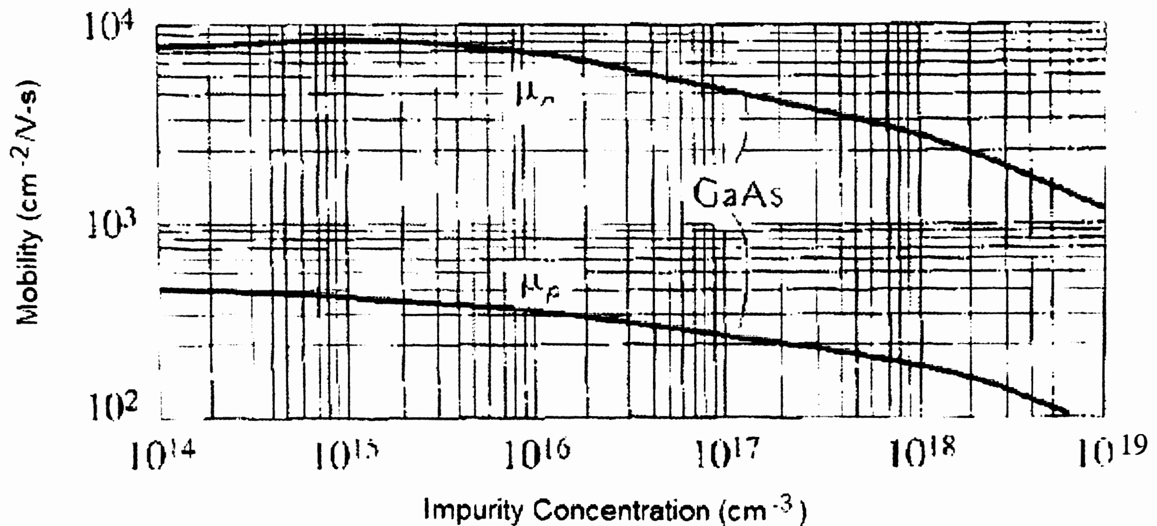

Figure 1.4. Electron and Hole mobility in relation to impurity concentration. Reference [6]

As it can be seen in the above graph, the electron and hole mobilities for GaAs are approximately one order of magnitude different from each other. Also notice that the mobility decreases as the carrier concentration increases. To make high quality material, the mobility and carrier concentration must be balanced. This will be discussed later along with the difference in operating modes for Hall devices.

Hall measurements and devices are quite often used to measure the mobility of materials. This is easy to see from Eq. 1.12. Once the mobility has been calculated, the carrier concentration can be determined from Eq. 1.3 resulting in the graph in Fig. 1.4. Knowing the mobility and carrier concentration gives a good characterization of the material used in the Hall devices. A Hall measurement and mobility calculation are also quite often used in measuring transistor characteristics.

For this project it was determined that the most efficient method of comparing different devices would be to create a sensitivity measurement. The sensitivity for this

project was defined as the output voltage divided by the applied magnetic field, divided by the bias current passing through the device. Eq. 1.13 relates the change in the Hall voltage to the change in the magnetic field the device sees from Eq. 1.12.

$$S = \frac{\Delta V_H}{\Delta B} = \mu_n \frac{W}{L} V_{bias} = \frac{I_{bias}}{qnt} \tag{1.13}$$

To be able to appropriately compare multiple devices, a general sensitivity was determined from Eq. 1.13. The general sensitivity is S divided by the bias current in the device.

$$S' = \frac{\Delta V}{\Delta B \cdot I_{bias}} = \frac{1}{qnt} \tag{1.14}$$

When looking at the sensitivity of a Hall device, there are two methods of measurement. The sample can be operated with a constant bias current or a constant bias voltage. As Eq. 1.13 shows, when the device is operated in constant voltage mode, using V_{bias}, the sensitivity is most affected by the electron mobility. From the constant voltage mode, it is clear that a very high μ_n is desired. A high μ_n allows for a lower V_{bias} when operating the device. A lower operating voltage is important in many cases where there are constraints on the amount of voltage that can be supplied to the circuit.

When the device is operated in the constant current mode, using I_{bias}, the carrier concentration (n) and thickness (t) are the driving factors. To keep the sensitivity high, the *nt* product from Eq. 1.13 must be examined. The *nt* product is often defined as the sheet concentration, n_s. The sheet concentration is the density of electrons. To have a highly sensitive material in constant current mode, the n_s must be as small as possible. From these two modes of operation, it becomes very obvious that the mobility and carrier concentration

must be balanced to obtain the most sensitive device. Using one operation method over the other does not significantly change the performance of the device, but does change the analysis. To see the different analysis methods take a closer look at the sensitivity of a device in constant current mode.

Looking at a constant current mode device, use the very right part of Eq. 1.13. The change in sensitivity dependent upon temperature can be found.

$$\frac{dS}{dT} = \frac{I_{bias}}{qt}\frac{d}{dT}\left(\frac{1}{n}\right) = -\frac{I_{bias}}{qt}\frac{1}{n^2}\frac{dn}{dT} \tag{1.15}$$

From this analysis, it is evident that the change in sensitivity with temperature originates from the change in the electron concentration with temperature. To see how the sensitivity changes in constant voltage mode, use the other part of Eq. 1.13.

$$\frac{dS}{dT} = V_{bias}\frac{W}{L}\frac{d\mu}{dT} \tag{1.16}$$

From the above equation, it appears that the sensitivity change is dependent upon the change in mobility with temperature. The difference between the two modes of operation comes about from the temperature dependence of the each. As the temperature increases, the mobility generally decreases. On the other hand, as the temperature increases, the carrier concentration generally increases. The two modes of operation change how the sensitivity of the device changes with temperature. However, the two modes of operation only affect the sensitivity slightly, and they can both be related to carrier concentration of the material. This is where the balance, as discussed before, comes in. The material must have the right amount of dopant to give as high a mobility as possible, but not too much so that the carrier

concentration increases too much. Balancing these two factors produces the best device independent of the mode of operation. Knowing how Hall devices work, one of the main objectives of the project can be examined.

1.3 Currently Available Technology

For this project one of the goals was to make devices that are comparable to those which can be purchased from companies within the industry. Table 1.1 shows the types and characteristics of Hall devices that could have been purchased commercially at the time of this project.

Table 1.1: Commercially available devices

Company	**Model #**		**Sensitivity**		**Material**
		Given Units	Supp. Cur.	V/A·T	
AKE	105A	6.25V/T	5mA	1250	InSb
AKE	108A	10.48V/T	5mA	2096	InSb
AKE	106A	2.71V/T	10mA	271	GaAs
FW Bell	BHT-910	1.1mV/KG	100mA	0.11	In
FW Bell	BH-704	7.5mV/KG	100mA	0.75	InAs
FW Bell	BH-204	11mV/KG	100mA	1.1	InAs

From [11-16]

This table lists the sensitivity the company provided for a specific current applied to the device. These measurements were used to calculate the sensitivity as it was previously defined for this project. As it can be seen from this table, the types of devices that were fabricated at Iowa State University are only directly comparable to the last four devices. The top two devices, which are made of indium antimonide, could be used as the ideal device for the final sensitivity measurements. InSb devices were not grown at ISU due to lack of

experience in material growth. InSb is also a much more difficult material to grow then InAs and GaAs.

Another measurement that should be taken into consideration when comparing these devices is the temperature stability of the devices. Assuming that the devices made at ISU will be used in the final probe design they must be able to withstand temperatures that will vary depending on which part of the country the probe is being used in. For example if the probe is being used in Arizona it must be able to withstand temperatures higher than 120°F. A probe being used in Maine must be capable of withstanding temperatures lower than -20°F. To understand the temperature stability of commercial devices the following graphs were obtained from the respective data sheets.

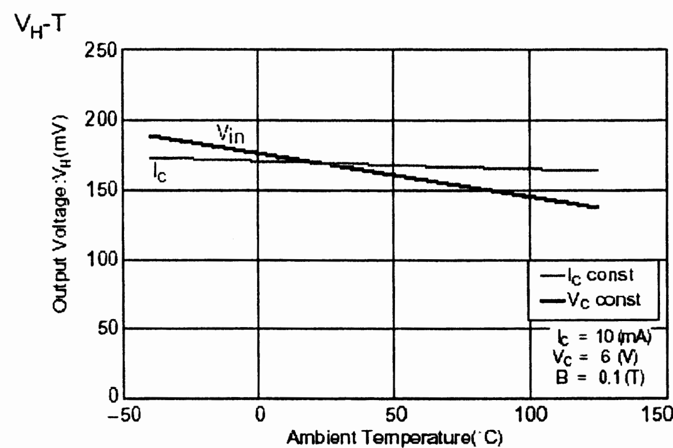

Figure 1.5. AKE model # HB-106A. From [13]

Figure 1.5 shows the typical temperature sensitivity a GaAs sample made by Asahi Kasei Electronics (AKE). As one can see, GaAs devices are much more temperature-stable devices

than the InSb samples made by AKE. The temperature sensitivity of InSb is shown in Fig. 1.6 below.

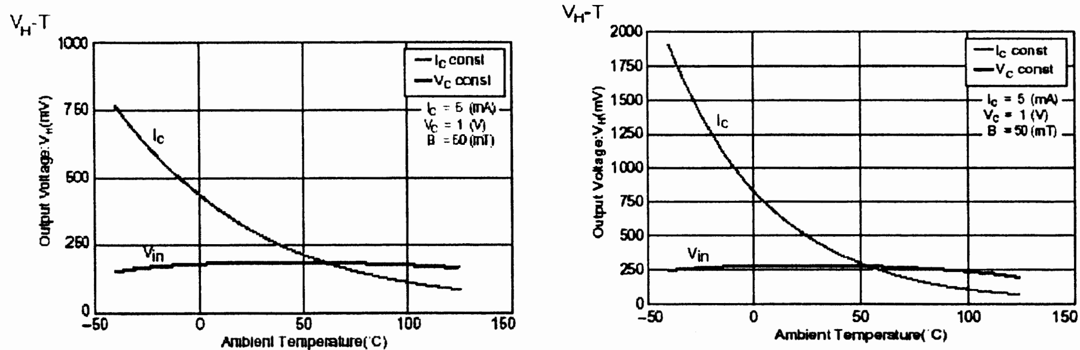

Figure 1.6. AKE model # HB-105A and HB-108A respectively. From [11], [12]

F.W. Bell gives temperature sensitivity measurements for their Hall devices--model # BHT-910--as ±50 PPM/°C when the controlling current is held constant and the temperature range is from –20°C to 80°C. Their InAs sample, model # BH-704, is listed as having a mean temperature coefficient of –0.04%/°C. This data is taken in the same temperature range and with the same parameters as the previous model number. The last sample used for comparison is the HB-204, which has a mean temperature coefficient of –0.08%/°C. Now knowing what rages of sensitivity we are aiming for the growth of our materials can be examined.

1.4 Material Growth

All samples for this project were grown in a molecular beam epitaxy (MBE) system. An MBE system must have an extremely low vacuum. Without a vacuum on the order of 10^{-10} Torr, so many particles are left in the chamber that the deposition of high quality

materials becomes very difficult. As with any epitaxial system, the more foreign particles in the chamber during deposition, the more impurities there will be in the material being grown or deposited. A schematic diagram of a MBE system is shown in Fig. 1.7.

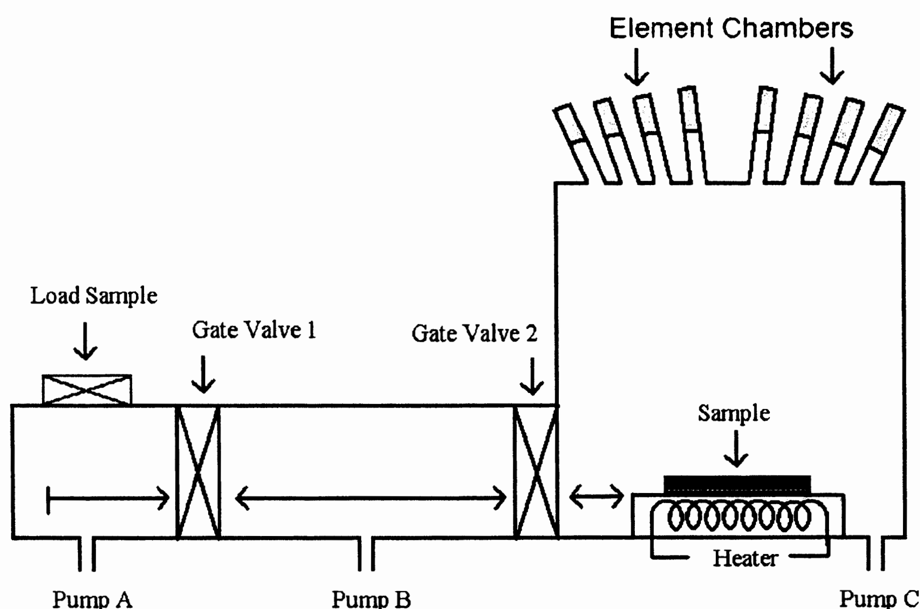

Figure 1.7. Simple MBE system schematic.

As Fig. 1.7 shows, there are three main chambers in the MBE system. The first chamber is where the sample is loaded into the system. This section is pumped down to a pressure of 10^{-6} Torr or lower with pump A. Once at the proper vacuum, gate valve 1 is opened and the sample is transferred into the second section. Here, pump B takes over and reduces the vacuum of only the second chamber to a pressure of 10^{-9} Torr or lower. Once at that pressure, gate valve 2 is opened, and the sample is transferred into the deposition chamber. Pump C then takes only the deposition chamber down to a pressure of 10^{-10} Torr. Before the materials can be grown, the sample must be heated. This removes any oxide on the sample that may be protecting the surface and promotes material growth.

To actually grow a specific material such as GaAs, there must be both Ga and As in the respective elemental chambers, shown opposite the sample in Fig. 1.7. These materials are then heated in a Knudson cell to produce an evaporating beam of the material. The beams then impinge on the substrate where surface mobility allows them to move into proper lattice positions. For III-V materials this growth progresses very well because the column III materials generally adhere well to the substrate, and column V materials generally do not have very high sticking coefficients. For a GaAs sample the Ga sticks to the surface more readily then As. It hits the surface of the substrate and finds the most energetically favorable position and stays there. Arsenic atoms generally will not stick to the hot sample surface, unless there is a free Ga atom that the As can bond to. The MBE system is capable of growing very high quality crystalline materials because of these properties. For this project the main types of materials that were used are bulk GaAs and an InAs quantum wells (QW).

GaAs and InAs QW are being used for this project because there is much experience in growing these materials at ISU. We did not grow InSb since it is a difficult material to work with, and we do not have experience with InSb growth. The bulk GaAs samples are very simple. The substrate is intrinsic GaAs so the lattice constant is the same for both the substrate and the active material. The bulk GaAs is then grown directly on top of the insulating substrate. For the bulk GaAs to be conductive it must be doped. The dopant that was used during growth was silicon (Si). Using Si to dope the GaAs makes the bulk GaAs an n-type material. Fig. 1.8 is a cross-sectional diagram of the GaAs samples grown in the MBE system.

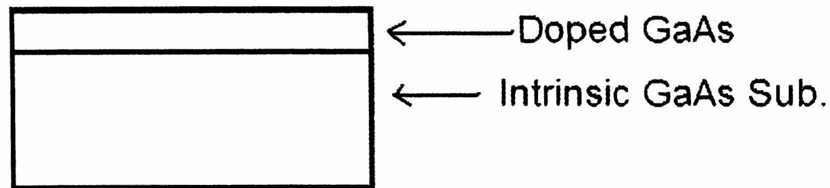

Figure 1.8. Bulk GaAs.

For the InAs QW samples, the process uses aluminum antimonide (AlSb) as the barriers of the QW [7]. The quantum well is used to control the sheet concentration of the material. The barrier layers confine the carriers to the InAs layer. Confinement does not change n much, while the thickness is greatly decreased. The adjustment of these two parameters keeps the sheet concentration low, which helps increase the sensitivity of the material in constant current mode. Using InAs QW we should be able to grow material with a sheet concentration of approximately 10^{12} cm^{-2}. This would increase the sensitivity of the material greatly as opposed to that of GaAs. The cross-sectional layer diagram shows the many layers that are grown to adjust the lattice constant of the AlSb so that it matches that of the GaAs substrate.

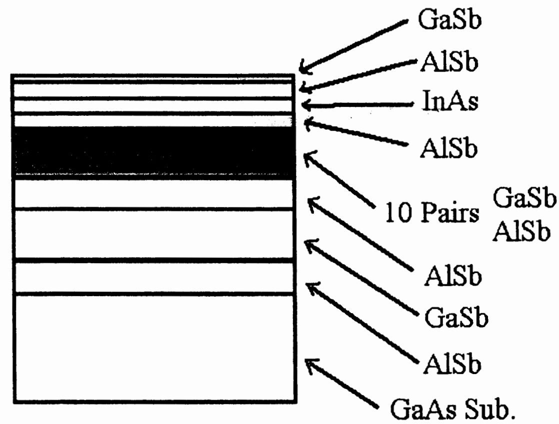

Figure 1.9. Typical InAs QW structure.

The first few layers are thicker layers so when the first material is grown on the substrate, it strains itself to adjust for the different lattice constant of the substrate. As the layer gets thicker, the new material tries to adjust itself back to its original lattice constant. The thinner layers are required to make the final adjustment from GaAs to AlSb so that the lower barrier layer for the Quantum well is not strained. Once it is understood how these samples are made, they can be examined for their electronic properties.

CHAPTER 2: DEVICE PATTERNS

2.1 First Set of Masks

To be able to test the material grown in the MBE system, there must be some type of device made. Fig. 2.1 shows two specific shapes of devices used for testing. On the left is a Hall bar and on the right is a van der Pauw device. The different shades of color represent different layers of the process. The blue layer represents the metal contacts, while the red layer represents the active device layer. To shape the material into the desired devices, photolithography is used.

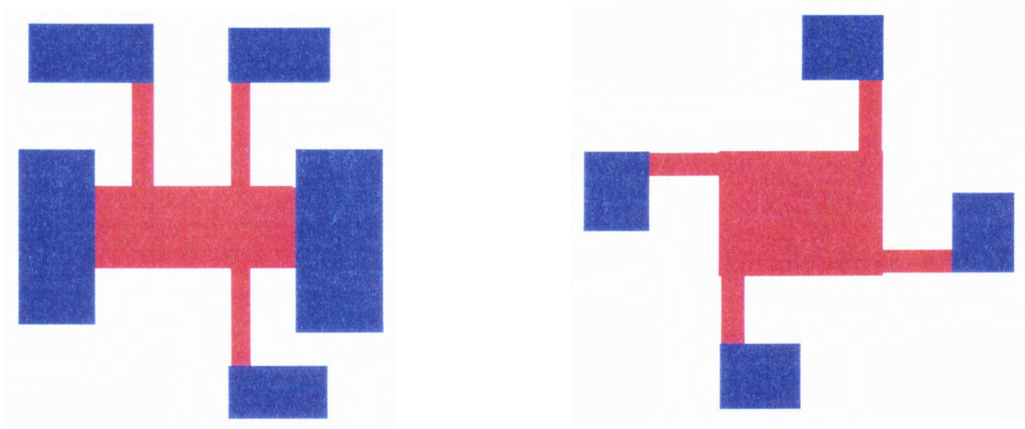

Figure 2.1. Hall bar and van der PAUW devices.

Using the van der PAUW theory, which allows for measurement of Hall voltages in an arbitrary shape, the device was planned to have a square shape. The necessary shape of a Hall bar is rectangular; therefore, that device shape was determined by theory. The Hall strip is an adaptation of the Hall bar, so its shape is also determined by theory. The Hall strip will be discussed later.

To form these shapes, a mask was developed for the lithography process. A layout program (tanner L-Edit) was used to create the mask file. The layout was created to get the maximum use out of each sample grown and to fit onto the smallest possible sample. The devices also had to remain large enough to make good contacts. For these reasons it was decided to make the layout fit within a one-centimeter by one-centimeter area for the van der PAUW and Hall bar devices. The sample size for the Hall strip was determined by the preliminary probe size being built by the NDE department.

The L-Edit program is used to make a layout of how the mask will appear, layer by layer. After determining device sizes and overall mask size, the masks in Fig. 2.2 were made. Picture (a) shows the mask pattern for van der PAUW and Hall bar samples. Picture (b) shows the mask layout of the Hall strip.

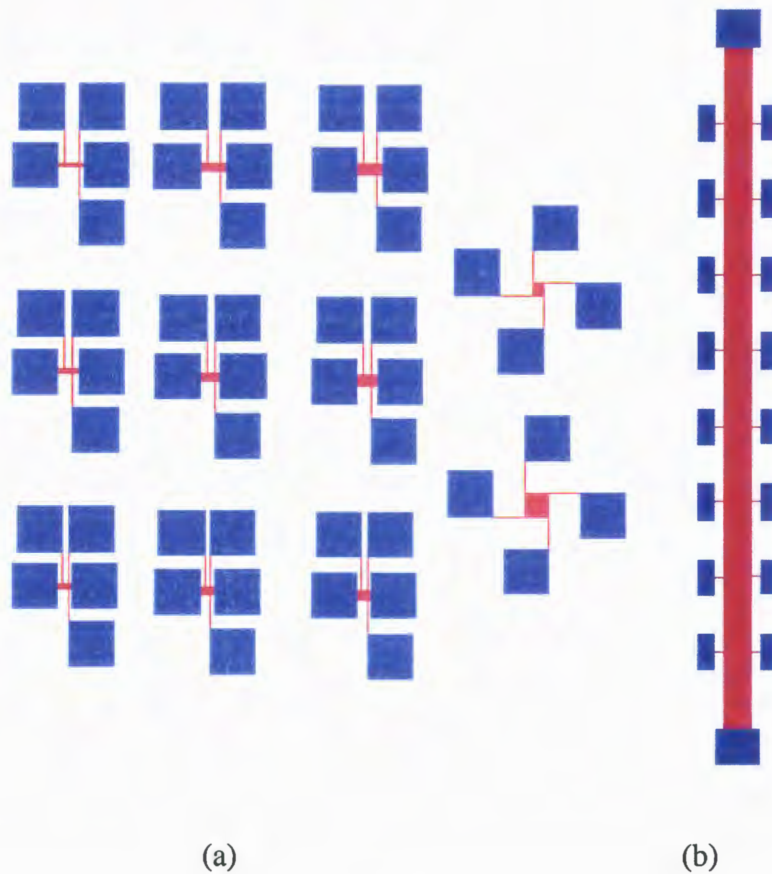

(a) (b)

Figure 2.2. Initial masks for van der PAUW, Hall bar, and Hall strip devices

In the mask containing the van der PAUW devices and Hall bars, there are two different van der PAUW devices to insure the calculations are independent of size. When testing the Hall bars, there are nine different sized devices so that two can be compared in such a way that only one of the dimensions is changed. This can be done for each dimension: length, width, and distance between Hall voltage points. The Hall strip was designed to fit into the NDE probe and to have eight points of contact to take eight Hall voltage readings. The dimensions of the devices in Fig. 2.2 are shown in Table 2.1, corresponding to the devices numbered in Fig. 2.3.

Table 2.1: First mask set dimensions

Device measurements from L-edit All units in microns

Device #	L	W	S	Pads	Bars to pads
1	400	100	200	750x750	12x400
2	400	150	200	750x750	12x400
3	400	200	200	750x750	12x400
4	300	100	150	750x750	12x400
5	300	150	150	750x750	12x400
6	300	200	150	750x750	12x400
7	200	100	100	750x750	12x400
8	200	150	100	750x750	12x400
9	200	200	100	750x750	12x400
10	200	200	-	750x750	12x400
11	400	400	-	750x750	12x400
Strip	18160	800	2000	500x1000	20x200
Strip end pads				1200x1000	

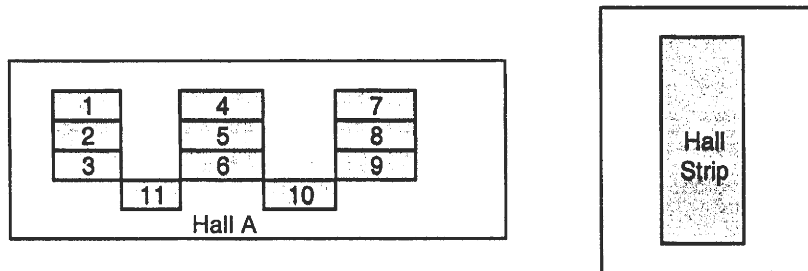

Figure 2.3. First mask set device dimension chart.

2.2 Second Set of Masks

While patterning the InAs quantum wells, it was found that the first set of masks contained parts of the devices that were too small for the etch to work properly. To solve this problem, a second set of masks was made with different dimensions. To make a mask set that was of maximum use, multiple sets of Hall devices were placed on one mask. For the second mask, design from the first mask set was adjusted so that the width of the bars that connect the Hall bar to the contact pads was made larger to compensate for the etch step of

the fabrication process. To make the set of devices easier to measure, the placement of the contact pads was adjusted in such a manner that the distance between each of the five contacts is identical for every device in the set. This allows for a single contact probe to be made that will be able to contact all the devices within this set independent of their size. These devices can be seen in Fig. 2.4.

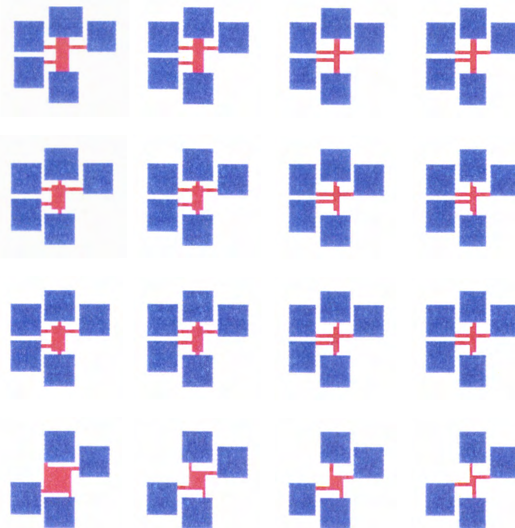

Figure 2.4. First group of devices from the second mask set.

As can be seen, this group has twelve Hall bars and four van der Pauw devices. In this group of devices, the size of the contact pads and the connection bars were minimized. Keeping the size of these parts of the device to a minimum allows for a large Hall bar that will fit within the designed coil area from the NDE probe. A full list of the Hall device dimensions is shown in Table 2.2.

Table 2.2: Second mask set dimensions

Device measurements from L-edit — All units in microns

Device #	L	W	S	Pads	Bars to pads(width)
1	1000	400	300	750x750	150
2	2000	400	700	750x750	150
3	1500	400	500	750x750	150
4	1000	500	300	750x750	150
5	2000	500	700	750x750	150
6	1500	500	500	750x750	150
7	500	200	200	450x450	20
8	375	200	150	450x450	20
9	250	200	50	450x450	20
10	400	400	-	450x450	20
11	500	150	200	450x450	20
12	375	150	150	450x450	20
13	250	150	50	450x450	20
14	300	300	-	450x450	20
15	500	100	200	450x450	20
16	375	100	150	450x450	20
17	250	100	50	450x450	20
18	200	200	-	450x450	20
19	500	150	150	450x450	20
20	375	150	50	450x450	20
21	250	150	100	450x450	20
22	100	100	-	450x450	20
strip	21000	800	2000	546x1092	136.5x214.5

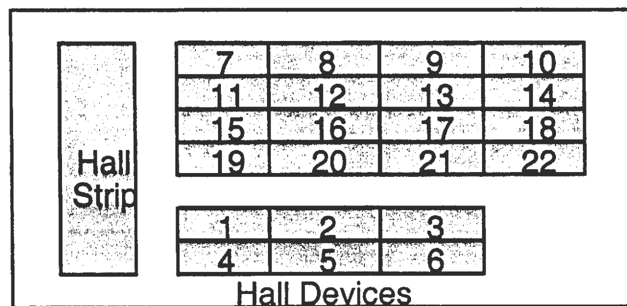

Figure 2.5. Second mask set device dimension chart.

The second group of devices on this mask set was made much larger in overall size. The main purpose of these devices was to make sure that the fabrication steps would work properly. The major difference from Fig. 2.4 and Fig. 2.6 are the dimensions. In Fig. 2.6 the bars from the Hall bar to the contact pads are 150 μm while the bars in Fig. 2.4 were 20 μm. This group of devices still fit within the one-centimeter by one-centimeter sample size as previously designed but only contain six devices instead of sixteen. A diagram of this group of devices is shown in Fig. 2.6.

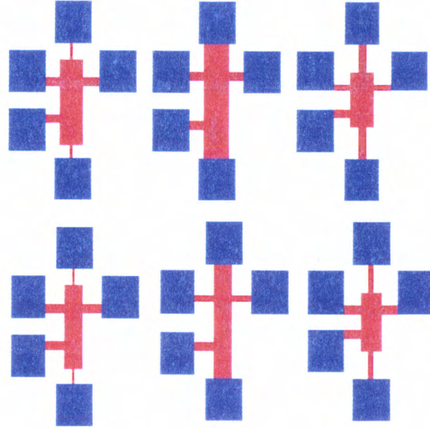

Figure 2.6. Second group of devices from the second mask set.

The third and final section of the second mask set was another Hall strip. For this device I used the first Hall strip device but changed the width of the bars that connect the contact pads to the device. The spacing between bars was held constant, and the bar was made longer to accommodate for the extra width in the bars. This device is shown in Fig. 2.7.

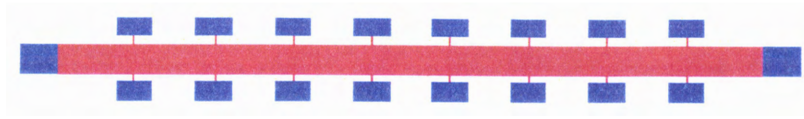

Figure 2.7. Third section from the second mask set.

After much initial testing, a final preliminary probe size was determined by the NDE department and a final mask was made with three sections.

2.3 Final Mask Set

The final mask contained two layers, the InAs QW structures and the metal contacts. The three sections of each layer consisted of a Hall strip, sixteen individual Hall bars, and a larger pair of Hall devices. The mask set is shown in Fig. 2.8.

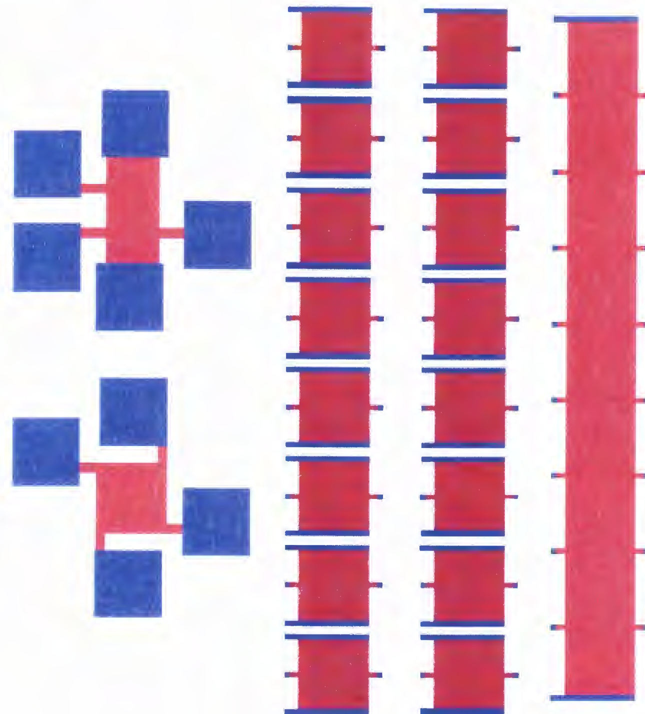

Figure 2.8. Final mask set of Hall devices.

The two larger devices are made so that they can be quickly tested. If they are working correctly the smaller devices are then tested. The two rows of eight devices are spaced and sized according to the constraints that were set by the probe designers in the NDE department. Each single row of eight devices is designed to be used in one probe. This would allow for two trials on each sample fabricated. The Hall strip is also designed to fit within the constraints given by the NDE department. For comparison reasons the Hall strip was designed with eight output voltage contacts. The dimensions of these devices are shown in Table 2.3.

Table 2.3: Final mask set dimensions

Device measurements from L-edit   All units in microns

Device #	L	W	S	Pads	Bars to pads(width)
1	1200	600	400	750x750	100
2	800	800	-	750x750	100
3	800	800	-	50x50	50
4	800	800	-	50x50	50
5	800	800	-	50x50	50
6	800	800	-	50x50	50
7	800	800	-	50x50	50
8	800	800	-	50x50	50
9	800	800	-	50x50	50
10	800	800	-	50x50	50
11	800	800	-	50x50	50
12	800	800	-	50x50	50
13	800	800	-	50x50	50
14	800	800	-	50x50	50
15	800	800	-	50x50	50
16	800	800	-	50x50	50
17	800	800	-	50x50	50
18	800	800	-	50x50	50
strip	7600	800	800	50x50	50

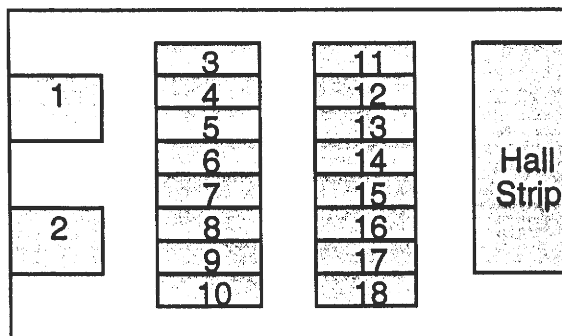

Figure 2.9. Final mask set device dimension chart.

CHAPTER 3: DEVICE FABRICATION

3.1 Fabrication process

Fabrication of the three different types of devices is nearly identical. The only change for each device is the respective mask. The more important change in processing procedures are the specific material steps. For example, the etching of different materials requires specific etching solutions. These techniques apply to both GaAs and InAs unless otherwise stated.

The first step in the fabrication process is the growth of bulk material on the substrate. The cross sectional view of the sample is shown in Fig. 3.1.

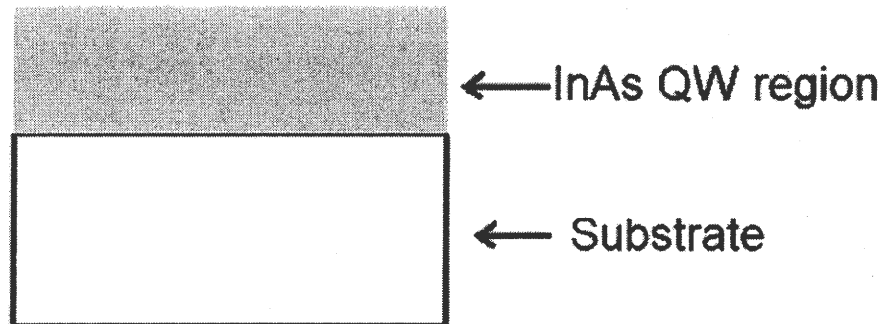

Figure 3.1. Cross sectional view of a sample after material growth.

The second step in the fabrication process is lithography to pattern the device region. Photoresist is spun onto the surface of the sample and then developed into the desired mask pattern.

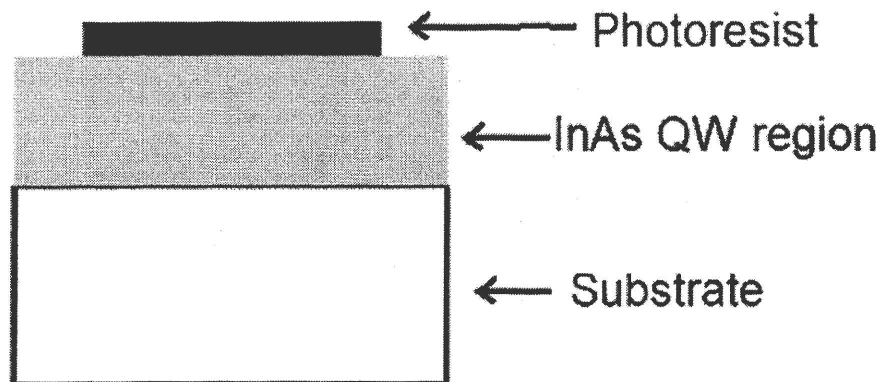

Figure 3.2. Cross sectional view of the first layer lithography process.

Next, the devices are etched using wet chemical etching, which will be discussed in more detail later. The results after the first lithography and etching are shown in Fig. 3.3.

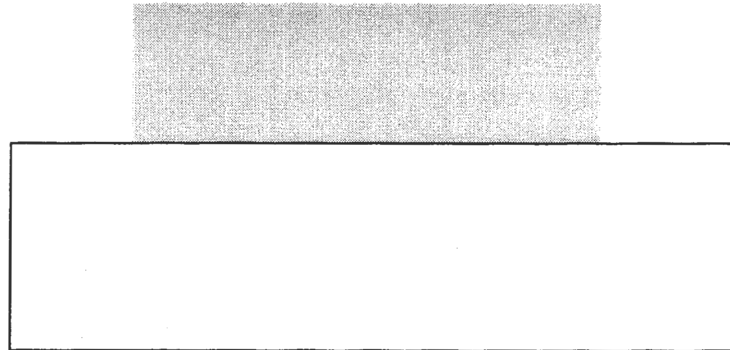

Figure 3.3. Cross sectional view of a device after etching and removal of the resist.

At this point in the process, the devices are ready for contacts. Depending on the desired types of contacts, temporary contacts can be made manually to the devices. If depositing permanent metal contacts, a second lithography step is needed. This process patterns the

metal being evaporated. A negative lithography process is used to pattern the photoresist in such a way to leave the contact pads exposed to the metal being deposited. The left half of Fig. 3.4 is a cross sectional diagram of the sample at this point in the fabrication. The grey regions, on the right in Fig. 3.4, represent the area of the hall device where the metal contacts were deposited. The black in the diagram represents the photoresist that has been placed on the sample and developed into the desired pattern. The evaporation and specific lithography process will be discussed later.

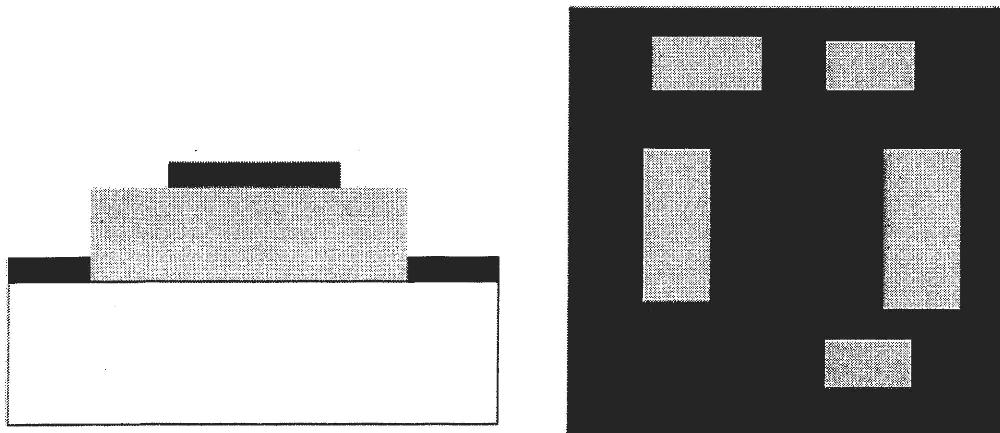

Figure 3.4. Cross sectional diagram after 2nd lithography process.

After depositing the contact layer, the unwanted metal and photoresist are removed; and the final devices with contacts can be tested.

3.2 First layer lithography

Once a mask set is designed and created, the process of fabricating the Hall devices from the bulk material can begin. The first step in the fabrication process is to place a pattern of the desired device shapes onto the bulk material. This was done with a Karl Suss MJB3

mask aligner. As a starting place for this process, the procedures outlined in the lab for the EE 432 microelectronics fabrication course at Iowa State University were used. These were obtained from the data sheet supplied by Clariant for a generalized positive tone process for use with the AZ 5200-E series photoresist [17].

Due to the fact that the resist adheres well to GaAs and GaSb, the dehydration bake and HMDS prime steps were eliminated. The lithography started with a spin coat of AZ 5214 E resist for 40 seconds at 4000 rpm's followed by a one-minute soft bake on a hotplate at 100°C. The next step was an ultraviolet exposure through the appropriate mask for 1.4 minutes. The final step before etching was a one-minute developing soak in MIF AZ 312 (1:1.2) developer for 60 seconds. An example of one of the InAs QW devices before etching is shown in Fig. 3.5.

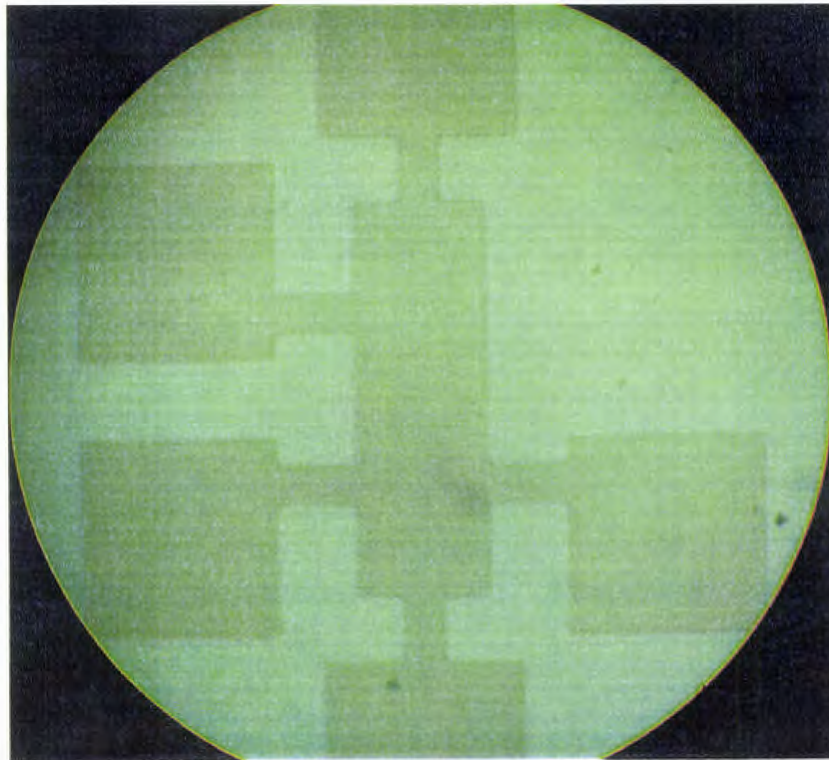

Figure 3.5. InAs QW pattern in photoresist before etching.

The darker green region of Fig. 3.5 is the patterned photoresist in the shape of a hall bar. The lighter green region is the surface of the bulk InAs QW. After the photoresist is patterned according to the desired device shape, the unwanted device material region must be etched away.

3.3 First layer etching

For the bulk GaAs samples, a wet chemical etching solution consisting of sulfuric acid (H_2SO_4), hydrogen peroxide (H_2O_2), and deionized water (H_2O) in a ratio of 1:1:8 was used [3]. The sample is placed in the etching solution and left until the surface of the sample appears similar to a GaAs substrate. The difference in the substrate and the devices can be easily seen due to the resist on top of the bulk GaAs material. To remove the resist after the etching is done, a simple acetone and methanol dip is performed in the respective order. The etching step is a critical step in the fabrication process. The reason it is so critical is that for every different material there can be very different wet chemical etches that work at different rates laterally and vertically. It is not safe to say that one specific etch will work for all materials.

For this reason a different wet etching solution was necessary for the InAs QW material. To etch the InAs QW, a solution of hydrofluoric acid, hydrogen peroxide, and deionized water was used. For the first attempt, a simple solution of $HF:H_2O_2:H_2O$ (1:1:10) was used. This solution etched through the InAs quantum wells very fast. It etched so fast that after a few samples were fabricated, it was determined that this strength of solution would not be appropriate for device fabrication. After many trials, it was also discovered that the etching solution was undercutting the devices more then desired. Undercutting occurs when the etching solution etches the devices pattern under the resist. After close

examination of the lateral and vertical etching of the HF:H_2O_2:H_2O solution, a new set of device dimensions was developed. These are shown in Fig. 2.8. After the second mask was completed and tested, the appropriate solution strength was determined to be 1:1:100 respectively. This strength of solution was found to etch at a rate that allows for complete device fabrication.

The difference in the appearance before and after etching is evident when comparing Fig. 3.5 to Fig. 3.6. Figure 3.6 displays the InAs QW device with a layer of photoresist on top of it. The photoresist is what is making the device green in color while the substrate is not green in color. The undercutting discussed before can also be seen in figure 3.6.

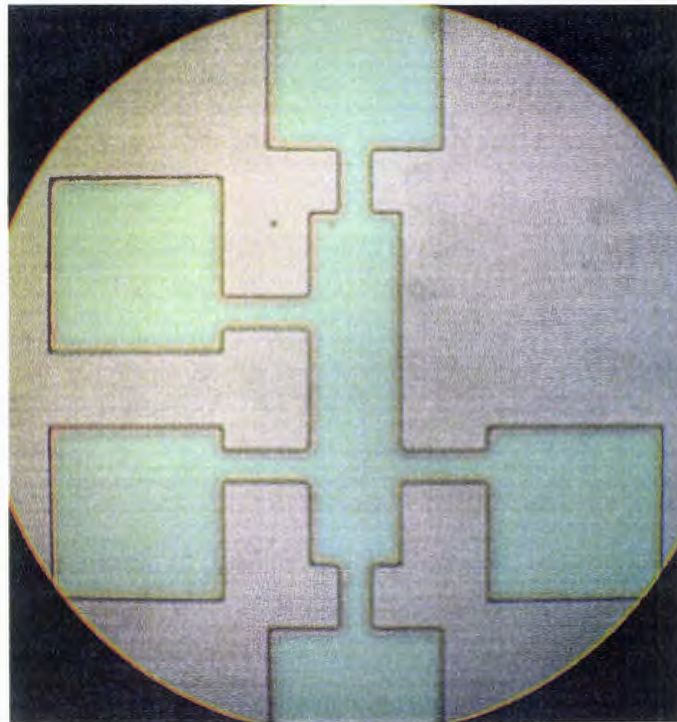

Figure 3.6. InAs QW device after etching and before removing resist.

To see the undercutting better, a picture was taken after zooming into an edge of the sample in Fig. 3.6. Examining the edges of the pattern show that the green color in the picture represent the active device area, but the outline does not follow the green pattern exactly. The difference in the green area and the outlined area is due to undercutting of the material.

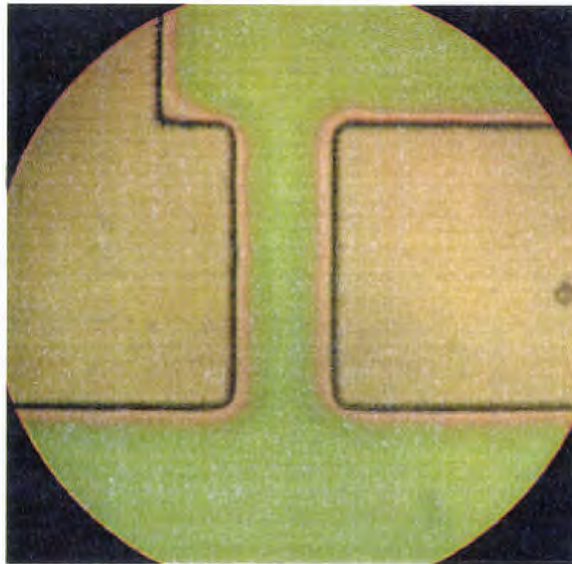

Figure 3.7. Undercutting effects on device patterns.

After examination of the device patterns, the resist is taken off the sample. At this point in the fabrication process, the devices are formed and isolated from each other. Once the first layer in the fabrication process was complete, the second layer or metal layer processing was developed.

3.4 Second layer processing, Metallization.

The second layer, metallization, forms the metal contacts on the surface of the hall devices. These contacts are necessary for permanent connections to be made in the final

probe assembly. Just as in the first layer, there are two different types of processes for each specific sample type. Due to the size of the contact pads and the possible use of multilayer metal contacts, a liftoff lithography process was best suited for this situation. The Clariant data sheets give a general negative lithography process for use with the AZ 5200-E series photoresist. The data sheets were used as a starting point in developing the process used to fabricate the metal contacts.

The masks for this process are shown in the figures in chapter 2. The blue parts of those figures represent the second layer of the masks. The first layer consists of the red sections of the figures. It is also important to note that the red sections extend below the blue sections so that the contacts are placed on top of active parts of the devices. The final list of process procedures is given below.

Second layer lithography steps

1. **DO NOT** Spin HMDS
2. Spin photoresist
    - o 4000rpm, 40 sec, AZ 5209E
3. Soft bake
    - o 1 min on hotplate at 100°C
4. Expose
    - o 1 min with metal layer mask
5. Reversal bake
    - o 1 min on hotplate at 120°C
6. Flood expose
    - o 5 min with Splice UV lamp Model # 5200-117V Serial # A651

   - o Place wafer on spinner and spin while exposing with lamp

7. Develop
   - o 1 min in developer DIL 1:1:2 MIF
8. Examine shapes to insure proper pattern for etching
9. Post bake: 125°C oven for 10-15 min (this step is optional)
10. Load samples into Evaporator for metal deposition

This process was established to be compatible with any metal that is desired for the contacts. After the photoresist has been put down and developed, the sample is ready for metallization. After the metal is evaporated onto the surface of the sample, the photoresist is removed by placing it in an ultrasonic acetone bath. The acetone will remove the photoresist and the metal on top of the photoresist. Leaving the metal on the desired contact pads only.

The combination of three layers: gold (Au), gold germanium (AuGe), and nickel (Ni) is a sufficient method of fabricating ohmic contacts on n-GaAs [3]. Once this process was discovered, the thickness of each respective layer was determined. The process consisted of first evaporating a layer of AuGe that was 200 Å thick. The second layer was a 100 Å thick layer of Ni, while the third and final layer of the contact was 1000 Å of Au. This same liftoff procedure was used for the contacts of the InAs quantum well structures.

Although the same liftoff procedure was used, a different set of metals was needed to acquire an ohmic contact to the QW devices. A two-step metal contact method consisting of 10 nm of Ti followed by 220 nm of Au was used [8]. The evaporation process was followed by an annealing step. A picture of an InAs QW device after final fabrication is shown in Fig. 3.8.

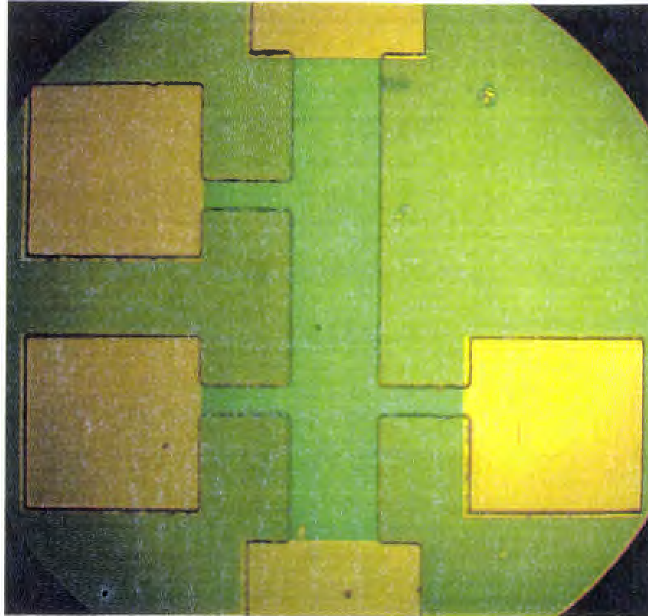

Figure 3.8. Final InAs QW device, sample 0306-1.

In this picture it is easy to distinguish between the three layers. The gold contacts pads appear gold in the picture while the active hall bar device appears green in Fig. 3.8. The dull green color in Fig. 3.8 is the substrate. Looking at the right most contact pad, the undercutting can be seen. The device contact pad should be the same size as the metal contact pad. As shown in Fig. 3.9 the device pad is slightly smaller than the metal deposited above it.

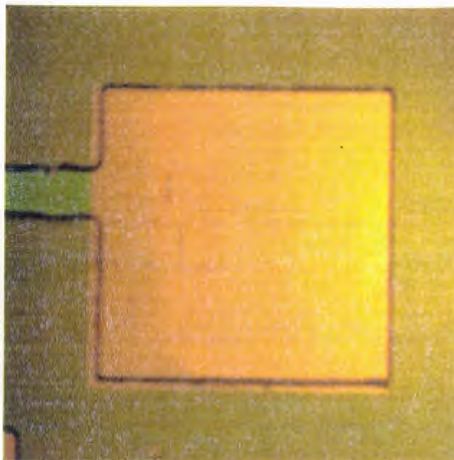

Figure 3.9. Ti/Au contact pad on an InAs QW device, sample 0306-1.

CHAPTER 4: TESTING OF DEVICES

4.1 Measurement Procedures

Once the three types of devices described in chapter 3 were fabricated, they were characterized. The characterization of the Hall bars and the Hall strip was very similar. The characterization of the van der Pauw (VDP) devices; however, was a bit different.

The VDP method describes the procedures for measuring the resistivitiy and Hall voltage of a flat sample of arbitrary shape [5]. The two most important requirements for the VDP method to be valid is the contacts need to be significantly smaller than the sample size and they must be located on the outer edge [5]. The final requirement of the VDP method is that there are no isolated holes in the sample [5]. An example of a VDP measurement is shown in Fig. 4.1. Using the four contacts shown in Fig. 4.1, A-D, and the resistivitiy of the material can be calculated.

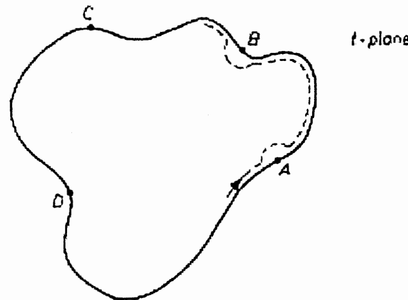

Figure 4.1. Van der PAUW measurement on a sample of arbitrary shape.

The resistivitiy is found by measuring the resistance of the sample two ways. The first resistance is calculated between contacts A and B in Fig. 4.1. To take this measurement the voltage is measured between contacts A and B while a current is passed between contacts C

and D. The second resistance is calculated between contacts B and C in Fig. 4.1. This measurement is calculated by measuring the voltage between contacts B and C while the current is passed between points A and D. The two resistance measurements, thickness, and a resistance dependent function are related to the resistivitiy of the sample in the manner shown by Eq. 4.1.

$$\rho = \frac{\pi d}{\ln 2} \frac{\left(R_{AB,CD} + R_{BC,DA}\right)}{2} f\left(\frac{R_{AB,CD}}{R_{BC,DA}}\right) \tag{4.1}$$

Calculating the resistance of the sample, as discussed before, and knowing the thickness are not the only requirements for finding the resistivitiy. The function, *f*, in Eq. 4.1 must also be calculated from the graph given by L. J. van der Paw in a Philips Research Report titled, "A Method of Measuring Specific Resistivitiy and Hall Effect of Discs of Arbitrary Shape." Knowing the resistivitiy and the thickness of the sample, the mobility, carrier concentration, and sensitivity of the material can be calculated. The mobility of the sample is determined by measuring the change in Hall voltage per change in magnetic field, multiplying by the thickness, and then dividing by the resistivitiy and current.

$$\mu = \frac{d\left(\frac{\Delta V}{\Delta B}\right)}{\rho I} \tag{4.2}$$

Equation 4.3 relates the carrier concentration of the sample to the inverse of the product of the mobility, the charge of an electron, and the resistivitiy of the sample. The sensitivity is calculated in the same manner as described in chapter 1.

$$n = \frac{1}{\mu e \rho} \tag{4.3}$$

The calculations involved in characterizing the Hall bars are discussed in chapter 1. To actually take the measurements on a Hall bar, the contacts are setup as shown in Fig. 4.2. The current is then passed through contacts A and D. The resistivitiy of the sample can be calculated by measuring the voltage between contacts B and C if there is no magnetic field present. The Hall voltage is taken between contacts C and E for specific magnetic fields.

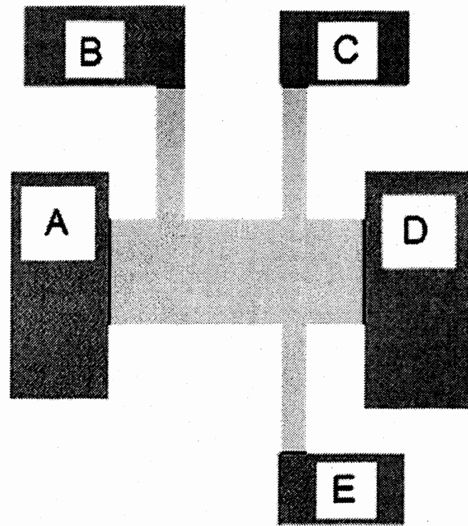

Figure 4.2. Hall bar conections.

Just as the connections in Fig. 4.2 are used to take the measurements for a Hall bar, they can also be used to take the measurements on a Hall strip. The main difference from the Hall bar and the Hall strip is that the Hall strip has eight sets of contacts. Groups of three contacts can be used in the same manner as shown in Fig. 4.2 to obtain all the necessary measurements to calculate the mobility, carrier concentration, and sensitivity of the Hall strip.

4.2 Measurement Apparatus

To be able to test various Hall effect devices, test equipment was needed. Two main pieces of equipment were missing from the Hemholtz coil system. The fist was a box of switches that would allow for testing of multiple types of Hall effect devices. The second was a piece of equipment to connect the box of switches to the sample.

It was decided that the set of switches would be adequate if it had the ability to test Hall bars, van der Pauw samples, and a Hall strip. To connect to each different device, the box had to be able to switch current and voltage probes on the sample. This was necessary to obtain all the data to calculate the sensitivity of the device. Looking at the Hall bar the box of switches can be configured to take measurements with minimal reconfiguration of connections between the sample and the box. The box of switches consists of five coaxial cables that connect to the sample, three manual switches, voltage connections, and a current connection. Figure 4.3 shows the box of switches, the current supply, the voltage meter, and Hemholtz coil magnets.

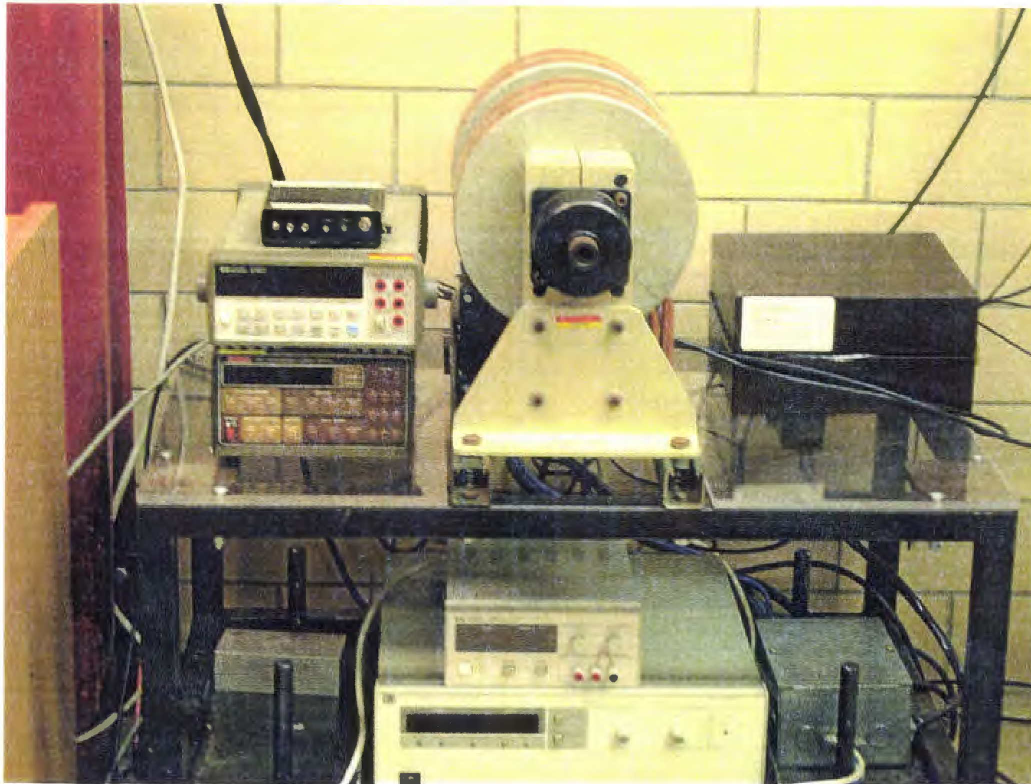

Figure 4.3. Hall test station.

The next piece of equipment that was needed was something to connect the sample to the testing apparatus. The connections from the sample holder to the sample were made with 0.001 mil gold wire. On one end of an aluminum box there were five coaxial connectors that are each connected to a copper square. This pad is where the gold wire is soldered to and then pressed into a dot of Indium (In) on the sample.

To properly take measurements, the five connections to the sample must be made at specific points on the sample. There are three different types of samples that can be connected to the box of switches. A list of standard operation procedures can be found in the appendix for this equipment.

The temperature stability measurements were taken in a very similar fashion. The main difference in the temperature measurements is the sample holder. The sample holder

used in these measurements was designed with a heater that, when supplied with a voltage, would heat the sample. The temperature of the heater was measured with a thermocouple and Hall measurements were taken as described previously.

CHAPTER 5: DEVICE CHARACTERIZATION

5.1 Fabrication Results

When developing devices from bulk material there are many different steps that must be examined. These steps have all been discussed in the previous chapters. In this chapter device characterization results will be discussed. The most difficult part of developing the fabrication process was determining what etching solution to use for each device material. As described in Chap. 3, the following solutions were used for each different device material.

Table 5.1: Etching solutions

Material	Solution	Strength
InAs QW	$HF:H_2O_2:H_2O$	1:1:100
GaAs	$H_2SO_4:H_2O_2:H_2O$	1:1:8

The next step in fabrication is the formation of contacts. To make quick temporary contact to all three types of devices, indium (In) foil was used. This foil was cut into small squares and placed on top of the device contact areas when using an appropriate mask. For each of the three materials, a permanent metal contact was electron-beam evaporated to a desired thickness. Table 5.2 shows the respective metal layers for each material.

Table 5.2: Metal contacts

Material	Contact Material	Thickness (Angs.)
InAs QW	Ti/Au	100/2200
InAs	Ti/Au	100/2200
GaAs	AuGe/Ni/Au	200/100/1000

To make sure the metal contacts were ohmic, part of the Hall device was used in an I-V test. For the contacts to be ohmic, they must display a linear I-V curve. This insures that the resistance of the contacts does not change with the current or voltage being supplied or measured through the contacts. The result of the I-V test for the GaAs devices is shown in Fig. 5.1.

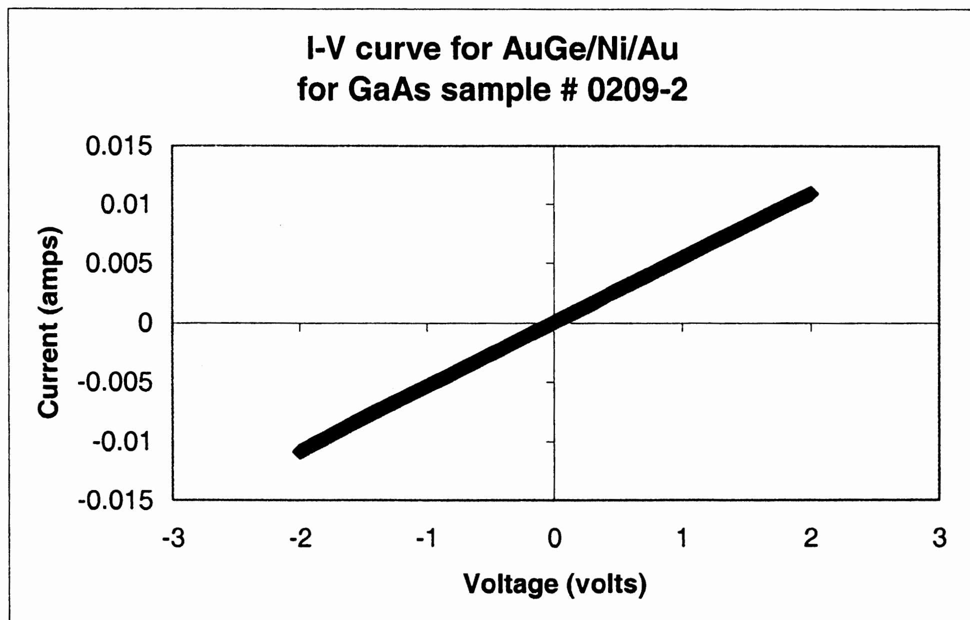

Figure 5.1: GaAs ohmic metal contact graph.

After characterization of this metal contact pad was done, further testing was also completed. The metal contact layer described above for the InAs QW was also tested. The results of the I-V test for the InAs QW device is shown in Fig. 5.2.

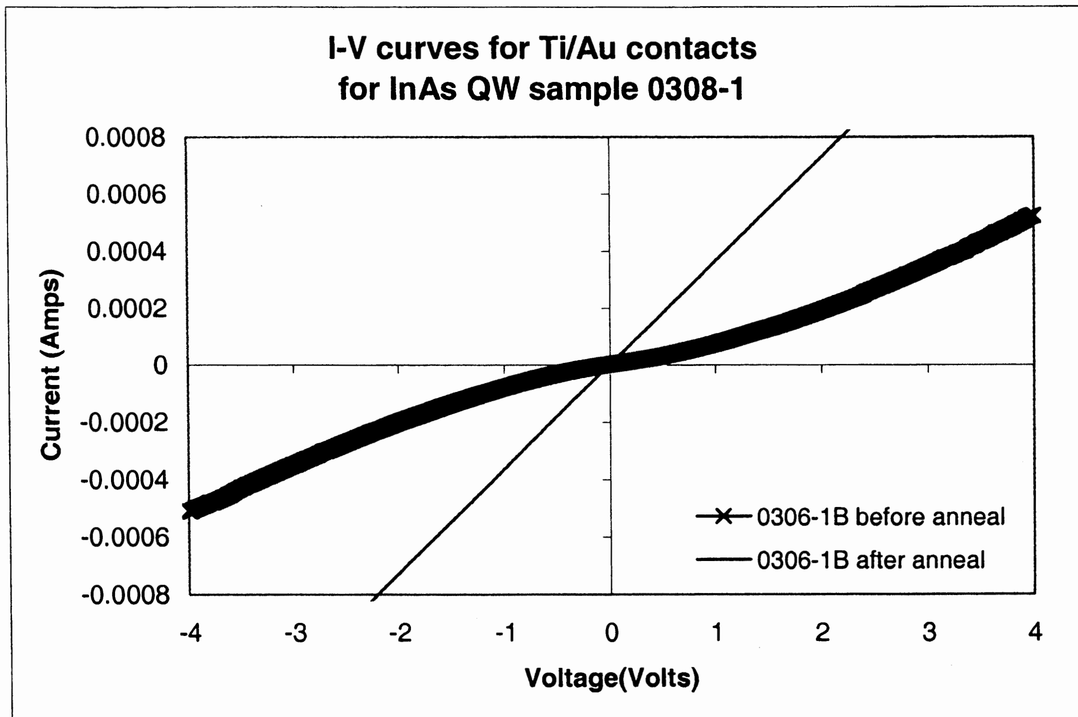

Figure 5.2: InAs QW ohmic metal contact graph.

The metal contact method required an anneal step to produce adequate ohmic contacts. The anneal step was done in a nitrogen ambient of 1 LPM at 300°C for 10 minutes.

5.2 Device Characterization Results

Knowing that the devices work and can be reliably connected, the actual device characteristics can be examined and compared to those obtained from commercial device data sheets. There are three main tests that were performed in determining the quality of the devices. The first test was a resistance test, which is necessary for calculation of the sensitivity of the devices. The other half of the sensitivity calculation is a Hall voltage test. The final test that was performed was the temperature dependence of the devices.

The resistance and Hall voltage tests were done with the testing apparatus discussed in Chap. 4. The GaAs sample that yielded the greatest sensitivity was sample # 0209-2. The rate at which the Hall voltage changes with the applied magnetic field is shown in Fig. 5.3.

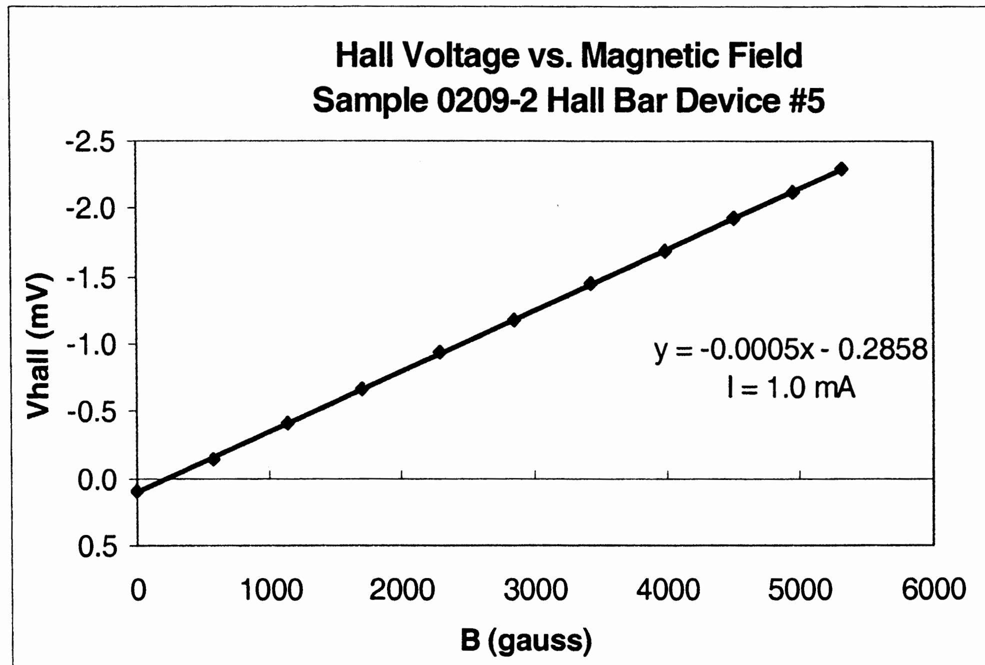

Figure 5.3: Output graph for GaAs sample 0209-2.

This data was taken at room temperature. To complete the characterization of the properties of GaAs Hall devices, the temperature stability of the devices was tested. To test the stability, the devices were supplied with 1.0 mA of current while in a magnetic field of 1137 gauss and 2284 gauss. This allows for calculation of $\Delta V/\Delta B$. The results are shown in Fig. 5.4. It is important while interpreting these results to understand how the error bars where calculated. These were calculated by finding the maximum deviation in the measured results above and below the average sensitivity of the results.

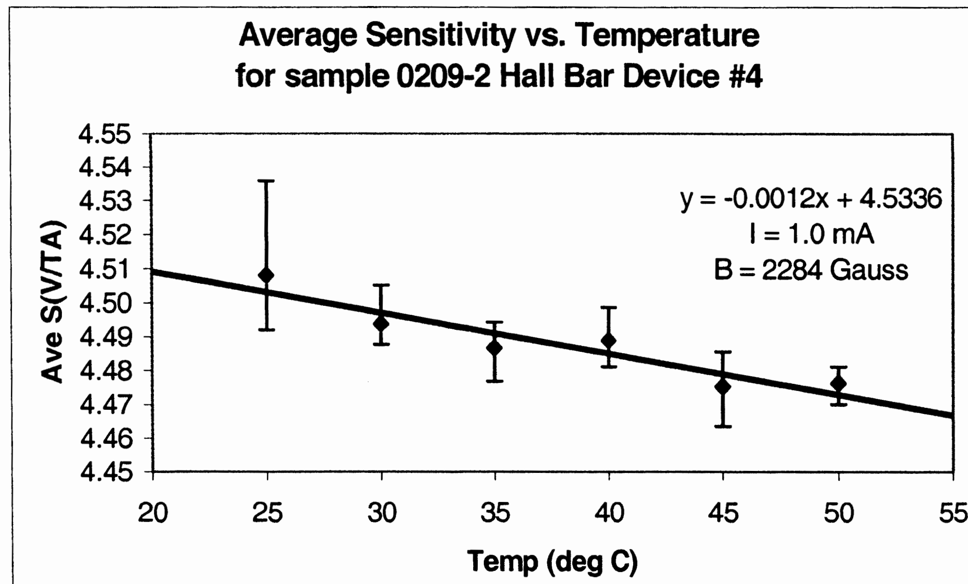

Figure 5.4: Temperature Sensitivity graph for GaAs sample 0209-2.

In examination of this graph it is important to notice that the sensitivity is changing at a rate of about 0.0012 V/A·T per degree C. This is a very small amount of change, which compares well with the data from the commercial devices. Just as the commercial devices display a flat temperature stability relationship, the microelectronics research center (MRC) devices also display relatively flat temperature stability. From the data in Fig. 5.3 the sensitivity as defined in Chap. 1 is determined. Sample 0209-2 yielded an average sensitivity of 4.58 V/ A·T, which deviates about 0.07 V/ A·T from the sensitivity at room temperature calculated in Fig. 5.4. From examination of commercially available devices, it was decided that the GaAs was not yielding high enough sensitivity, so work was begun with InAs quantum wells.

InAs QW were tested in the same manner as the bulk GaAs samples. To see the initial improvement in results, a graph of the Hall voltage versus the magnetic field is shown in Fig. 5.5.

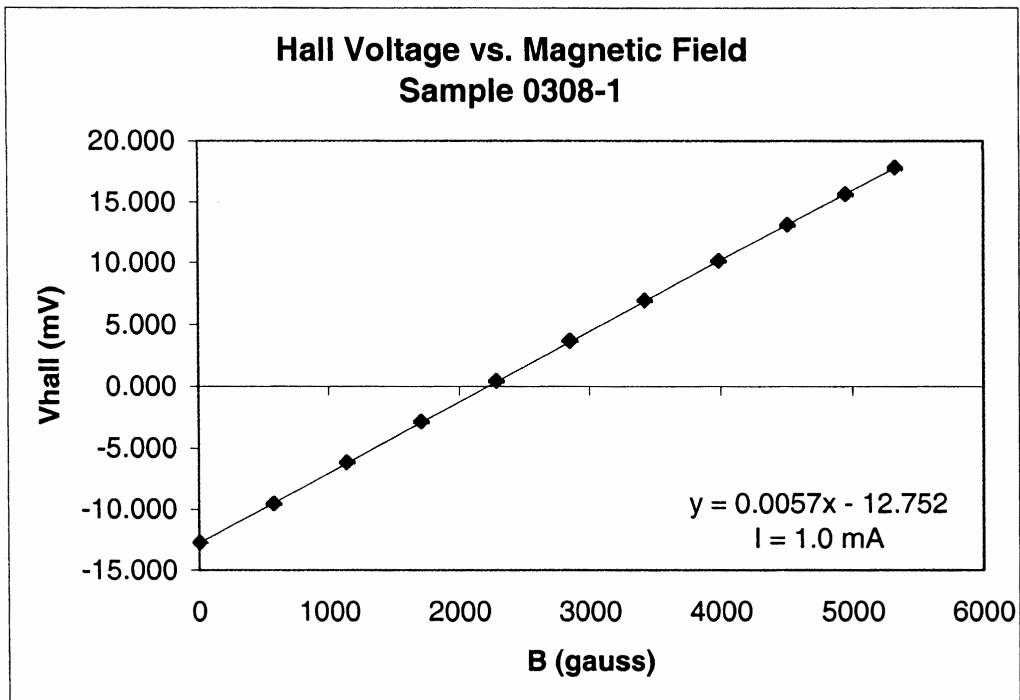

Figure 5.5: Output graph for InAs QW sample 0308-1.

This data was taken at room temperature. To demonstrate the confidence in these results, a large number of trials were taken with this single sample. From that data the error in measurements was determined, and the error bars are displayed on the above graph. The error bars are so small compared to the overall change in output voltage, they cannot be seen. Thus, yielding much confidence in this data. By comparing the slope of Fig. 5.3 versus Fig. 5.5, it is easy to see there is approximately a factor of ten increase in device quality. To take a closer look at the improvement, look at the sensitivity of this device. From the data used to create the graph in Fig. 5.5, the sensitivity was calculated to be 56.4 V/ A·T at room temperature. To further characterize this device, the stability of the device was tested as the temperature of the device was altered. Again multiple trials were taken with a single sample as to confirm reliability in the measurement. This data is shown in Fig. 5.6.

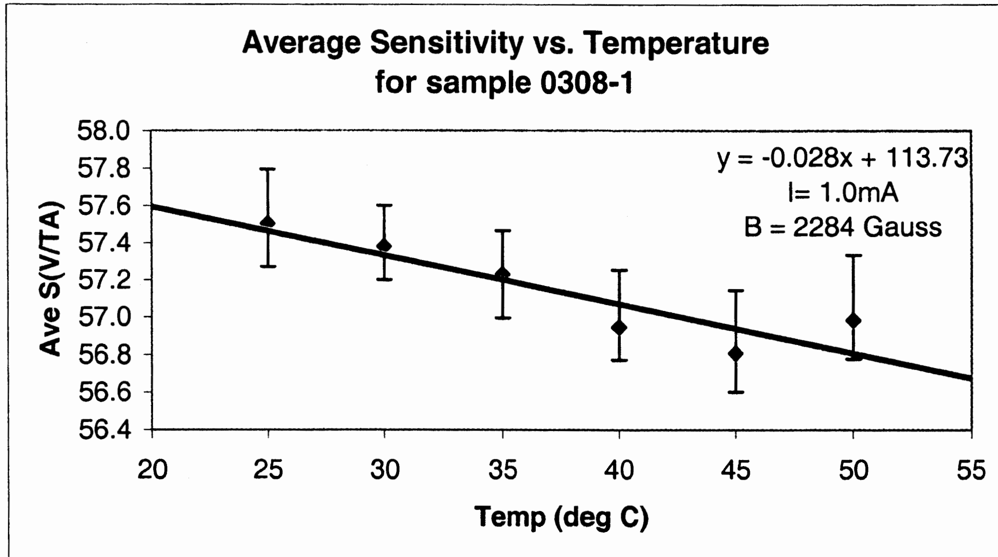

Figure 5.6: Temperature sensitivity graph for InAs QW sample 0308-1.

The graph above displays how the sensitivity of this device changes with temperature while also displaying the actual measured error, maximum above and below the average, from six trials. The most significant result to examine from this graph is the slope. This experiment shows that the sensitivity changes at a rate of about –0.028 V/ A·T per degree C. This compares very well with the change in sensitivity of commercially available devices. This is very comparable to the F.W. Bell InAs devices, which have a temperature coefficient of –0.04 %/°C. The shape of this graph can also be compared to the shape of the graphs in Fig. 1.6. Notice that the InSb stability, in constant current mode, varies much more than this InAs QW, which also varies much more then the GaAs devices.

5.3 Hall Array Results

Once the individual devices had been fabricated and tested, Hall strips were fabricated and tested. A Hall strip was fabricated using material from sample 0209-2. A

Hall voltage measurement was taken for each pair of contacts along the Hall strip. The results are shown in Table 5.3.

Table 5.3. Sample 0209-2 Hall strip results.

Hall voltage pair	μ_H (cm^2/Vs)	n (cm^{-3})	S'(V/AT)
1	2782.678	6.47E+17	4.83
2	2728.851	6.67E+17	4.69
3	2697.650	6.82E+17	4.58
4	2649.633	7.01E+17	4.46
5	2672.215	7.13E+17	4.36
6	2616.204	7.27E+17	4.29
7	2594.998	7.36E+17	4.24
8	2567.217	7.44E+17	4.20
ave	**2663.681**	**7.02E+17**	**4.46**

The average sensitivity along the Hall strip compares well with the overall average sensitivity measured for all devices fabricated on sample 0209-2, which was 4.58 V/ A·T. From Tbl. 5.3 it is also important to notice that each pair of Hall voltages produced results that were not dependent upon the nearest pair. Therefore, each pair along the Hall strip acted as an individual Hall bar would have acted. This result is very encouraging since a Hall strip can be used in place of individual Hall bars in an array. The main advantage of the Hall strip is that the pairs of Hall voltage connections can be placed much closer to each other then they could if individual Hall devices were being used. There are also fewer connections to be made on a Hall strip than on a corresponding number of Hall bars. In theory, the closer together the Hall voltages are taken, the more accurate and sensitive the array will be.

5.4 Conclusions

Being able to fabricate a Hall strip at ISU allowed for tight positioning of the Hall sensors in the desired positions. This would not have been possible if Hall devices had been

purchased commercially. From the above results the Hall strip is shown to act in the same fashion as the corresponding number of independent Hall devices, thus reducing the number of contacts wires needed in the final probe. In any probe the fewer wires and number of contacts that need to be dealt with the easier the probe is to work with. The individual Hall devices fabricated showed similar advantages.

The fabrication of an array of individual Hall devices onto one substrate allowed us to put more devices in the same area then would have been possible with commercially available devices. The most significant result is the sensitivity of the devices when compared to commercial devices.

Table 5.4. Sensitivity comparison chart.

Company	Model #	Sensitivity(V/AT)	Material
AKE	105A	1250	InSb
AKE	108A	2096	InSb
AKE	106A	172	GaAs
FW Bell	BHT-910	0.11	In
FW Bell	BH-704	0.75	InAs
FW Bell	BH-204	1.1	InAs
ISU MRC		4.58	GaAs
ISU MRC		56.4	InAs QW

Table 5.4 shows the actual sensitivity results from devices created at ISU and the sensitivity of similar devices available commercially. A quick comparison of the GaAs samples shows that the ISU MRC devices were not nearly as high quality as commercial devices. The lower sensitivity and the desired range of sensitivity shown by the InSb devices was the driving factor in working with InAs QW. Using quantum wells to control the sheet concentration allowed us to fabricate Hall devices with a much greater sensitivity than current InAs commercial devices. Although the InAs QW was an improvement over the GaAs, our InAs

QW sensitivity was not on the same order as the InSb devices made by AKE. To see if there is more potential for these devices compare the theoretical mobility to the actual measured mobility.

Table 5.5. Mobility comparison chart.

Material	Theoretical μ	Experimental μ
GaAs	8000	2690
InAs QW	10000	5247

Table 5.5 shows the theoretical and experimental mobilities in $cm^2/Vsec$ for the materials grown at Iowa State University. From this table it is evident that more work can be done to continue to improve the quality of materials being grown in the MBE system.

5.5 Future Work

Just as this project did more work is needed to continue to improve the materials grown at ISU. A higher quality material will result in improved mobility and device sensitivity. Improvements in material quality can be examined, as could the growth of InSb in the MBE system at ISU. Along with improving the material more work can be done on fabrication of the devices. To improve the etching of the devices reactive ion etching could be explored as a substitute for wet chemical etching. This would eliminate the undercutting of the devices. Eliminating the undercutting would then allow for reconfiguration of the devices contact pads and overall device sizes. Improving the device sizes would then allow for a larger array to be fabricates and tested. A first improvement to the array size would be to increase the number of devices from 8 to 16 and then possibly 32. As the number of devices in an array increases the area of the sample being examined by the probe will

increase, which could then increase the efficiency of the probe. Improving the device dimensions and further examination of the space between devices could allow for a greater image to be generated from a stressed sample. An examination of a two dimensional array could also be done. A two dimensional array might give the imaging process an even greater view of cracks in metal components. Overall as more work is done to improve the devices used in the probe the more reliable the detection of defects in components will be. Therefore, the components used after inspection will be much safer then if inspected with current methods of nondestructive evaluation.

APPENDIX. BLACK BOX S.O.P.

Procedures for using Hall measurements box and sample holder.

This black box and sample holder will test the resistivitiy and measure the Hall voltage of both a Van der Pauw sample and a Hall bar.

Step 1: place sample in sample holder
  If connecting a Van der Pauw use diagram 2, if connecting a Hall bar use diagram 1 (left or right which ever is similar to your device).

Step 2: Connect sample to terminals (yellow wires) using gold wire according to the kind of sample testing.

Step 3: Connect numbered terminals on sample holder to corresponding numbered terminals on black box.

Step 4: Connect voltmeter to black box.

Step 5: Connect current source to black box.

Step 6: Plug black box into wall outlet (make sure the tip of the power cord is positive).

Step 7: Set switches 1, 2, and 3 according to the measurement desired.

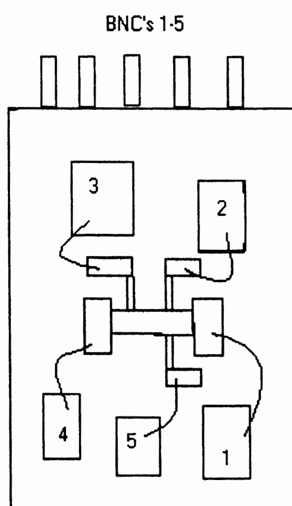

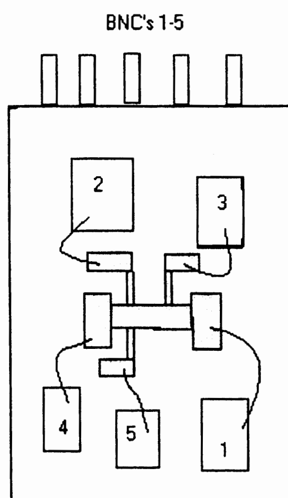

Diagram 1

Diagram 2

Switch settings for Van der Pauw and Hall Bar measurements

Switch	**1**	**2**	**3**	**Measurement**
Position	Down	Up	Up	Van der Pauw resistance
Position	Down	Down	Down	Van der Pauw and Hall Bar resistance
Position	Up	Down	Down	Van der Pauw Hall (in magnetic field)
Position	Up	Up	Up	Hall Bar Hall measurement (in magnetic field)

REFERENCES

[1] Jiles, David, Introduction to Magnetism and Magnetic Materials. Second Edition. Chapman & Hall, London. 1998.

[2] Plummer, James D.; Deal, Michael D.; and Griffin, Peter B. Silicon VLSI Technology Fundamentals, Practice and Modeling. Prentice Hall, Upper Saddle River, NJ. 2000.

[3] Williams, Ralph E. Gallium Arsenide Processing Techniques. Artech House, INC, Dedham, MA. 1984

[4] Diefenderfer, A. James; Holton, Brian E. Principles of Electronic Instrumentation. Third Edition. Saunders College Publishing, Philadelphia, PA. 1994.

[5] Van der PAUW, L.J. "A Method of Measuring Specific Resistivity and Hall Effect of Discs of Arbitrary Shape." Philips Research Reports 13, Eindhoven, Netherlands. 1-9, 1958.

[6] Neamen, Donald A. Semiconductor Physics & Devices. Second Edition. McGraw-Hill, Boston, MA. 1997.

[7] Tuttle, Gary. "Electron transport properties of InAs/AlSb quantum wells grown by molecular beam epitaxy." Doctor of Philosophy, University of California Santa Barbara, CA, U.S.A. Aug. 1991.

[8] Bolognesi, C. R.; Chow, D. H. "InAs/AlSb Dual-Gate HFET's" IEEE Electronic Device Letters. Vol. 17, No. 11,534-536. Nov. 1996.

[9] Johnson, Marcus. "Pulsed Eddy-current measurements for materials characterization and flaw detection." Doctor of Philosophy, University of Surrey, Guildford, Surrey, GU2 5XH, US. March 1997.

[10] Goldfine, Neil; Zilberstein, Vladimier; Shay, Ian; Schlicker, Darrell; Windolwoski, Mark; Washabaugh, Andrew (Jenteck Sensors, Inc.); Kollgaard, Jeff. "Multi-Site Damage Imaging of 3rd Layer Cracks in Lapjoints using MWM-Arrays." 6th Joint FAA/DOD/NASA Aging Aircraft, 2002. 16-19 Sept. 2002

[11] Asahi Kasei Electronics: InSb hall element model # HW-105A: data sheet. http://www.asahi-kasei.co.jp/ake/en/ms/pdf/hw105a.pdf (Date accessed: Nov. 10, 2003).

[12] Asahi Kasei Electronics: InSb hall element model # HW-108A: data sheet. http://www.asahi-kasei.co.jp/ake/en/ms/pdf/hw108a.pdf (Date accessed: Nov. 10, 2003).

[13] Asahi Kasei Electronics: GaAs hall element model # HW-106A: data sheet. http://www.asahi-kasei.co.jp/ake/en/ms/pdf/hg106a.pdf (Date accessed: Nov. 10, 2003).

[14] F.W. Bell 900 series hall sensor: Bulk Indium BH-900 series hall sensors: data sheet. http://www.sypris.com/library/documents/BH-900-Datasheet.pdf (Date accessed: Nov. 10, 2003).

[15] F.W. Bell 700 series hall sensor: Bulk Indium Arsenide BH-700 series hall sensors: data sheet. http://www.sypris.com/library/documents/BH-700-Datasheet.pdf (Date accessed: Nov. 10, 2003).

[16] F.W. Bell 200 series hall sensor: Bulk Indium Arsenide BH-200 series hall sensors: data sheet. http://www.sypris.com/library/documents/BH-200-Datasheet.pdf (Date accessed: Nov. 10, 2003).

[17] AZ 5200 I-Line Photoresist Data Sheet from Clariant. AZ Electronic Material ID: 9084293631. 30 May 2001.

ACKNOWLEDGMENTS

I would like to thank the members of my committee; Dr. Gary Tuttle, Dr. John Bowler, and Dr. Alan Constant; for giving me guidance and support throughout this process. The FAA for monetary support of the project I was involved with. To all those who helped me to get my research done by helping fix equipment or preparing equipment for use, you helped a great deal in the research process. I would also like to thank all the people who helped me brainstorm ideas and find solutions to problems. Last but not least, thank you to all my friends I've made through my time here at Iowa State University. Marcus Johnson, Haiyan Sun, Curtis Sell, Nee-Fong S, Jonathan Williams, Max Noack, Jason Muehlmeier, Wai Lung, David Garcia, Matt Ring, Josh Graves, Paul Seberger, Reagan Johnson, Jarrod McDonald, Matt Welch, Eric Weatherford